Colloidal analogs of molecular chain stoppers

Anna Klinkova[a,1], Héloïse Thérien-Aubin[a,1], Rachelle M. Choueiri[a], Michael Rubinstein[b,2], and Eugenia Kumacheva[a,c,d,2]

[a]Department of Chemistry, University of Toronto, Toronto, ON, Canada M5S 3H6; [b]Department of Chemistry, University of North Carolina at Chapel Hill, Chapel Hill, NC 27599-3290; [c]Department of Chemical Engineering and Applied Chemistry, University of Toronto, Toronto, ON, Canada M5S 3E5; and [d]The Institute of Biomaterials and Biomedical Engineering, University of Toronto, Toronto, ON, Canada M5S 3G9

Edited by David A. Weitz, Harvard University, Cambridge, MA, and approved October 11, 2013 (received for review August 13, 2013)

A similarity between chemical reactions and self-assembly of nanoparticles offers a strategy that can enrich both the synthetic chemistry and the nanoscience fields. Synthetic methods should enable quantitative control of the structural characteristics of nanoparticle ensembles such as their aggregation number or directionality, whereas the capability to visualize and analyze emerging nanostructures using characterization tools can provide insight into intelligent molecular design and mechanisms of chemical reactions. We explored this twofold concept for an exemplary system including the polymerization of bifunctional nanoparticles in the presence of monofunctional colloidal chain stoppers. Using reaction-specific design rules, we synthesized chain stoppers with controlled reactivity and achieved quantitative fine-tuning of the self-assembled structures. Analysis of the nanostructures provided information about polymerization kinetics, side reactions, and the distribution of all of the species in the reaction system. A quantitative model was developed to account for the reactivity, kinetics, and side reactions of nanoparticles, all governed by the design of colloidal chain stoppers. This work provided the ability to test theoretical models developed for molecular polymerization.

nanopolymer | plasmonic properties

The similarity between chemical reactions and colloidal self-assembly forms a bridge between molecular and colloidal length scales, spanning over several orders of magnitude (1–3). It is currently well-established that a broad range of particles with two reactive patches, such as polymer microbeads (4), inorganic nanoparticles (5), and block copolymer micelles (6), act similar to bifunctional molecular monomers and organize themselves into one-dimensional polymer-like structures. The self-assembly of colloidal polymers can also be assisted by the application of an electric (7) or magnetic field (8). The analogy between chemical reactions and the self-assembly process offers a mutually beneficial approach: (*i*) the use of synthetic concepts as a strategy for controllable and quantitative self-assembly of colloidal particles into structures with well-defined sizes, spatial organization, and directionality and (*ii*) the development of fundamental knowledge about chemical reactions by visualizing colloidal assemblies.

The replication of synthetic concepts developed at the molecular scale—beyond qualitative prediction of a particular structure—should benefit the self-assembly of colloidal polymers built from nanoparticles. Collective plasmonic, excitonic, and magnetic properties of nanoparticle chains depend on their degree of polymerization (9–11). Nanoparticle chains have potential applications as sensors (12), nanoantennas (13), or waveguides (14), to name just a few applications, and their successful realization relies on the ability to precisely control nanopolymer structure. Recently, we reported the ability to predict the average degree of polymerization $\overline{X}_n$ of nanoparticle chains for a particular self-assembly time (5); however, without quenching the self-assembly after an appropriate time, the desired final value of $\overline{X}_n$ cannot be achieved. Synthetic polymer chemistry offers an elegant way to tune $\overline{X}_n$ by changing the stoichiometry of reacting molecules. For monomers with two functional groups A and B, the value of $\overline{X}_n$ is controlled by adding to the reaction system a small amount of monofunctional molecules that are called chain stoppers (CSs) (15). In the course of polymerization, a CS attaches to the polymer end and makes it incapable of further reaction. The value of $\overline{X}_n$ of the polymer is tuned by varying the amount of CSs introduced in the reaction system. This efficient approach has not been explored for controlling the degree of polymerization (or the length) of colloidal polymers.

Importantly, the ability to visualize individual nanoparticles and their ensembles, and analyze their distribution in the system brings a unique capability to take snapshots of different stages of colloidal polymerization reactions and in this manner, test theoretical models developed for synthetic polymer chemistry. For example, supramolecular polymerization uses bifunctional monomers and CSs with identical, self-complementary functional groups (16). Control of $\overline{X}_n$ of supramolecular polymers has been developed under the assumption of equal reactivities and strengths of CS–CS, CS–monomer, and monomer–monomer interactions (16–18). Side reactions of CSs such as their dimerization and binding to the junctions between the repeat units of the polymer have been neglected. Direct characterization of supramolecular polymers is not trivial due to their dynamic nature, and conventional polymer characterization techniques, e.g., gel permission chromatography, may require dilution of polymer solutions or the use of elevated temperatures, which can change polymer properties (16). Visualization of nanoparticle chains by electron microscopy in the course of the polymerization process enables the validation of the assumptions made for CS reactions and, overall, provides insight into the intrinsic details of supramolecular polymerization, although nanopolymer chains are generally characterized by a lower value of $\overline{X}_n$ than their molecular counterparts. Furthermore, nanoscience-specific techniques

Significance

Self-assembly of nanoparticles in polymer-like chains bears a strong similarity to polymerization reactions, in which monomer units are brought together by directional noncovalent interactions. Based on this similarity, the molecular concepts of polymer chemistry can be applied to achieve controllable nanoparticle assembly. On the other hand, the ability to visualize nanoparticle assemblies and to exploit characterization tools used in nanoscience offers a unique way to study polymerization reactions. Here we explore this twofold strategy for an exemplary system including the self-assembly of bifunctional metal nanorods in the presence of monofunctional nanoparticles (chain stoppers). The approach provided insight into the polymerization kinetics, side reactions, the distribution of species in the system, and the design rules for the synthesis of molecular chain stoppers.

Author contributions: A.K., H.T.-A., and E.K. designed research; A.K., H.T.-A., and R.M.C. performed research; A.K., H.T.-A., M.R., and E.K. analyzed data; and A.K., H.T.-A., M.R., and E.K. wrote the paper.

The authors declare no conflict of interest.

This article is a PNAS Direct Submission.

[1]A.K. and H.T.-A. contributed equally to this work.

[2]To whom correspondence may be addressed. E-mail: mr@unc.edu or ekumache@chem.utoronto.ca.

This article contains supporting information online at www.pnas.org/lookup/suppl/doi:10.1073/pnas.1315381110/-/DCSupplemental.

such as the measurements of time-dependent red shift of surface plasmon resonances of metal nanoparticles can be used to characterize their polymerization in linear chains. Importantly, the design rules established for efficient colloidal CSs can be extended to the synthesis of their molecular analogs to control reaction kinetics and the distribution of molecular species in the reaction system.

The present work highlights mutual enrichment of nanoparticle self-assembly and polymerization reactions. We designed colloidal analogs of molecular CSs with a particular geometry and surface properties to achieve control of their reactivity, minimize the effect of the side reactions of CSs, and fine-tune the value of $\overline{X}_n$ of polymers formed from bifunctional gold nanorods (NRs). We proposed a quantitative model that—based on the reaction kinetics—quantitatively predicts the value of $\overline{X}_n$ and the relative concentrations of all of the species in the reaction system, all controlled by the intelligent design of CSs. These results provide an important contribution to supramolecular polymerization.

Results and Discussion

Rational Design of the Colloidal CSs. Fig. 1 illustrates polymerization of bifunctional Au NRs in the presence of monofunctional CSs. The NRs are end-tethered with thiol-terminated polystyrene (PS) molecules which form a "bush" at each NR end. The organization of the NRs in chains is mediated by reducing the quality of the solvent for the PS ligands. Following the addition of water to the solution of NRs in dimethylformamide (DMF), a good solvent for PS molecules (19), the NRs assemble in an end-to-end manner to minimize the surface energy of the system. When a CS attaches to one or two ends of the NR chain, the polymerization process is suppressed or completely stopped, respectively.

We devised the following critical design rules for the colloidal CSs.

Surface chemistry. The ligands capping two distinct patches of CSs render colloidal stability to the nanoparticles before the beginning of the self-assembly. When the self-assembly of the NRs is initiated, the reactive ligands selectively lose their solubility and form a physical bond with the NR end (Fig. 1). The ligands attached to the reactive and nonreactive patches are sufficiently short to avoid the screening of the counterpart segment.

Dimensions of reactive and nonreactive domains of CSs. To cap the NR end and avoid the attachment of multiple CSs, the size of the reactive patch of CSs should be complementary to the diameter of the NR, whereas the size of the nonreactive patch of CSs should be moderately larger than the NR diameter. The latter feature introduces steric hindrance against the attachment of multiple CSs to the NR end and controls CS reactivity, both in polymerization and side reactions such as their dimerization and bonding with chain junctions. In addition, CS reactivity is controlled by the geometry of the nonreactive segment blocking access to the reacted surface for potential "bonding partners," e.g., additional CSs or NRs.

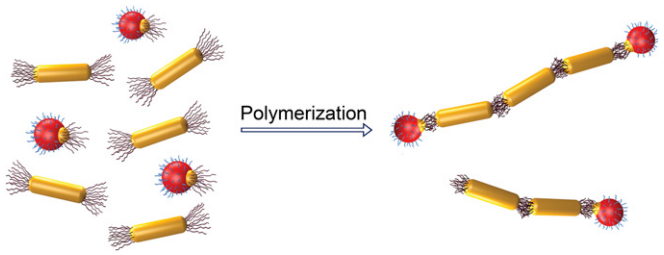

Fig. 1. Self-assembly of bifunctional Au NRs in the presence of monofunctional CSs. Yellow and red correspond to the reactive (Au) and nonreactive (Fe_3O_4) patches of CSs, respectively.

Synthesis and Surface Modification of CSs and NRs. We synthesized Au NRs with a mean length and width of 35 nm and 10 nm, respectively (Fig. 2*A*), as reported elsewhere (20), and subjected them to ligand exchange to replace cetyltrimethylammonium bromide at the {111} facets on the NR ends with PS molecules (M_n = 5,000 g/mol) (21). Fig. 2*B* shows CSs comprising Au and Fe_3O_4 domains (labeled in Fig. 1 with yellow and red, respectively), which were coated with oleic acid and oleylamine ligands (22). An insignificant fraction of CSs had a flower-like morphology, as shown in *SI Appendix*. The optimized diameters of the Au and Fe_3O_4 segments were 6.5 ± 0.9 nm and 15.4 ± 1.6 nm, respectively (Fig. 2*C*). The CSs were subjected to the two-step ligand exchange to cap the Au and Fe_3O_4 patches with thiol-terminated PS and dopamine-terminated polyethylene glycol molecules, respectively (2, 23, 24). The number average molecular weight of the PS ligands was 5,000 g/mol, similar to that used for end functionalization of the NRs, and the molecular weight of dopamine-terminated polyethylene glycol ligands was 1,200 g/mol. Following ligand exchange, the average hydrodynamic diameter of the CSs in DMF increased from 24 to 32 nm (Fig. 2*D*). The CSs were colloidally stable in DMF for at least 1 mo.

Self-Assembly Experiments. To verify the distinct surface chemistry of the Au and Fe_3O_4 patches after ligand exchange, we examined CS self-assembly in a solvent that was selective for either PS molecules, or for polyethylene glycol ligands. The CSs were dispersed in acetone, a good solvent for both the PS and polyethylene glycol, and either water or dioxane was added to this colloidal solution. In the acetone–water mixture (a poor solvent for the PS molecules) (25), the CSs assembled into dimers by forming a physical bond between the small, PS-coated Au domains (Fig. 2*E*). In the acetone–dioxane mixture, the quality of the solvent was reduced for polyethylene glycol (25). The CSs formed clusters containing several nanoparticles that were linked by the polyethylene glycol molecules (Fig. 2*F*). The clusters, rather than dimers, formed due to the large attraction area of reactive Fe_3O_4 patches and a small surface area of the stabilizing Au segments.

Next, we explored the CS strategy by introducing colloidal CSs at the ratio $0 \le [CS]/[NR] \le 1.55$ to the solution of Au NRs in DMF, where [CS] and [NR] are the molar concentrations of CSs and NRs, respectively. Subsequently, water was introduced in the mixed solution to achieve the target concentration C_w = 15 vol %.

We monitored the polymerization reaction by examining transmission electron microscopy (TEM) images of the monomers and colloidal chains at varying time intervals. Fig. 3*A* shows representative species observed in the DMF–water solution in the course of self-assembly: individual CSs and NRs (*Top*), dimers of CSs and noncapped NR chains (*Middle*), and NR chains end-capped with CSs at a single end and at both ends (*Bottom*). A fraction of CSs attached to the junctions between the ends of neighboring NRs in the chains (*Inset*).

The ability to visualize all nanoparticle species in the system enabled their detailed analysis and characterization. The schematics of free and reacted PS bushes attached to NRs and CSs and the change in their concentration in the course of self-assembly are shown in Fig. 3 *B* and *C*, respectively. The concentrations of free PS bushes attached to individual CSs and NRs were reduced due to the formation of CS–CS, CS–NR, and NR–NR bonds. Analogous to step-growth polymerization, the unreacted CSs and NRs were present in a relatively high amount in the entire range of self-assembly time t_{SA} in comparison with reacted nanoparticles (15). A limited number of CS dimers were formed, due to the low reactivity of CSs to each other (the rate

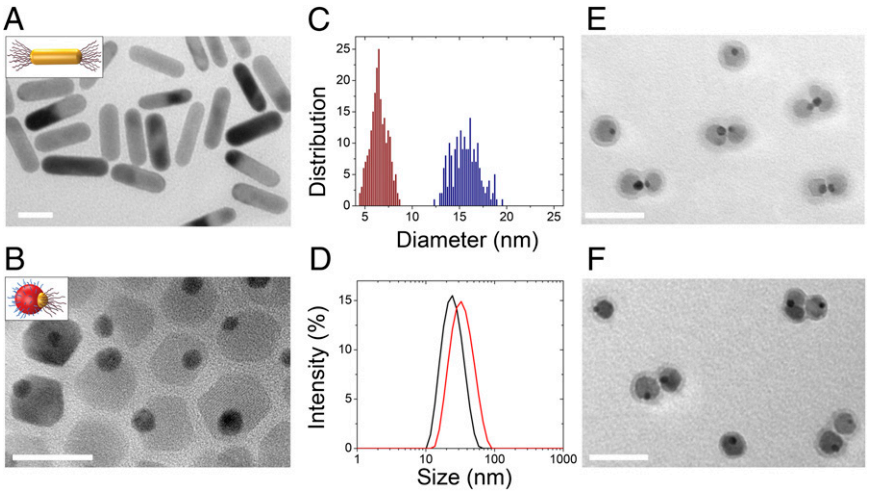

Fig. 2. CS approach to controllable self-assembly of colloidal polymers. (*A*) TEM image of Au NRs functionalized with polystyrene molecules (bushes) at both ends. (*Inset*) Schematic of bifunctional NR. (*B*) Au–Fe_3O_4 colloidal CSs capped with thiol-terminated polystyrene and dopamine-terminated polyethylene glycol molecules at the surfaces of Au and Fe_3O_4 domains, respectively. Dark and light regions correspond to the Au and Fe_3O_4 domains, respectively. (*Inset*) Schematic of the colloidal CSs. (*C*) Distribution of sizes of the Au and Fe_3O_4 domains (*see SI Appendix* for details). (*D*) Distribution of hydrodynamic diameters of Au-Fe_3O_4 CSs before (black curve) and after (red curve) attachment of polymer ligands to the surface of Au and Fe_3O_4 domains. (*E*) Self-assembly of CSs in acetone–water mixture at the content of water of 20 vol %. (*F*) Self-assembly of the CSs in acetone–dioxane mixture at the content of dioxane of 65 vol %. The time of self-assembly in *E* and *F* is 15 h. (Scale bars: *A* and *B*, 20 nm; *E* and *F*, 50 nm.)

constant was 0.03×10^{-3} $nM^{-1}{\cdot}s^{-1}$, in comparison with 2.3×10^{-3} $nM^{-1}{\cdot}s^{-1}$ for NR–NR addition). A weak contribution of CS–CS reaction was predesigned by the small (0.073) fraction of the reactive surface area of the Au patch, steric hindrance, and the geometry of the Fe_3O_4 domain. At the initial stage of self-assembly, the fraction of NR–NR bonds increased faster than the fraction of NR–CS bonds (the rate constants were 2.3×10^{-3} $nM^{-1}{\cdot}s^{-1}$ and 1.8×10^{-3} $nM^{-1}{\cdot}s^{-1}$, respectively). Importantly, at small t_{SA}, the attachment of CSs to the chain ends dominated over their attachment to the chain junctions; however, with an increasing number of junctions in the chains and a reducing number of chain ends, the side reaction of CSs with junctions could not be ignored.

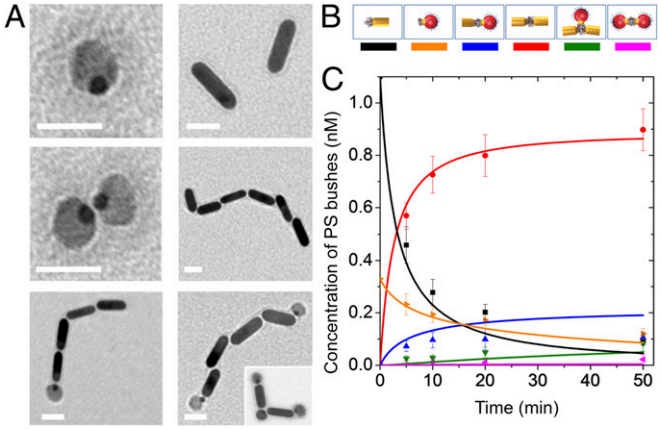

Fig. 3. Monitoring polymerization of NRs in the presence of CSs. (*A*) TEM images of representative nanoparticle species in the course of self-assembly. [CS]/[NR] = 0.6, C_w = 15 vol %, t_{SA} = 20 min. (Scale bar, 20 nm.) (*B*) Schematics of free and reacted PS functional groups (bushes). (*C*) Variation in the concentration of PS functional groups in the course of self-assembly for nanoparticle species shown in (*B*). [CS]/[NR] = 0.6. Symbols correspond to the experimental data obtained from TEM image analysis; the lines correspond to the numerical solution of *SI Appendix*, Eqs. **S9–S12**. Error bars indicate SD. The colors in *C* correspond to the colors of bars in *B*.

End-to-end assembly of Au NRs leads to electrodynamic coupling between the alternating dipoles along the chain (26). In our experiments, a time-dependent red shift of the longitudinal surface plasmon resonance $\Delta\lambda_{LSPR}$ of the self-assembled NR chains was substantially weaker in the presence of CSs than in the control CS-free system (Fig. 4*A*). We used the value of $\Delta\lambda_{LSPR}$ to monitor NR self-assembly in the presence of different amounts of CSs (Fig. 4*B*). Increase in the ratio [CS]/[NR] led to a strong decrease in the rate of change and the magnitude of $\Delta\lambda_{LSPR}$. For example, for [CS]/[NR] = 1.55, a red shift of only 6 nm was observed for t_{SA} = 60 min, in comparison with 147 nm measured for [CS]/[NR] = 0. (We note that the plasmonic resonance of CSs was centered at 550 nm, and thus did not interfere with $\Delta\lambda_{LSPR}$.) The decrease in $\Delta\lambda_{LSPR}$ was related to the reduction in the average number of NRs in the chains, which was in agreement with earlier findings (27).

Fig. 4*C* shows the variation in the average number of NRs in the chains defined as $\overline{X}_n = \frac{\sum n_i x_i}{\sum n_i}$, where x_i is the number of NRs in the chain and n_i is the number of chains containing x_i NRs. In CS-free system, the value of $\overline{X}_n$ increased linearly with time, following the trend of reaction-controlled step-growth polymerization, in agreement with earlier findings (5); however, in the presence of CSs the linear variation of $\overline{X}_n$ vs. t_{SA} did not hold, as the growth of NR chains was suppressed by the attachment of CSs. For instance, for t_{SA} = 20 min, in the absence of CSs, $\overline{X}_n$ = 8.2 was measured, whereas at the ratio of [CS]/[NR] = 1.55 the value of $\overline{X}_n$ of only 1.5 was achieved.

Modeling of Self-Assembly. We developed a quantitative model for the self-assembly of bifunctional NRs in the presence of colloidal CSs. The model describes comprehensively the variation in $\overline{X}_n$ with t_{SA} and NR conversion, predicts the maximum value of $\overline{X}_n$ achieved at a particular CS concentration, provides the distribution of the fractions of all reactive species in the system, including CSs lost to side reactions, and accounts for the reactivity and rate constants of nanoparticles forming CS–CS, CS–NR, and NR–NR bonds. The details of modeling are included in *SI Appendix*.

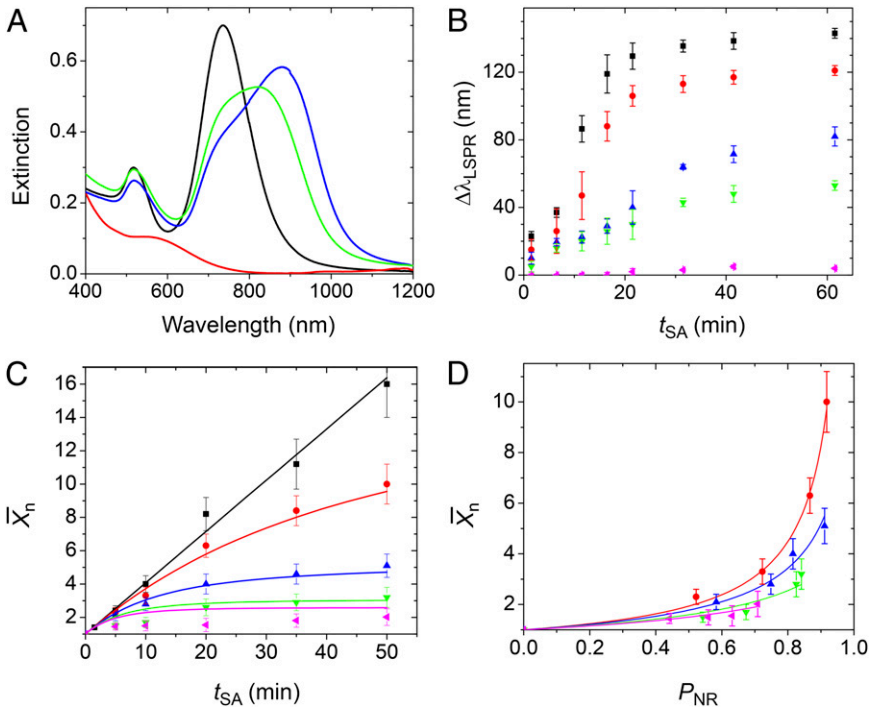

Fig. 4. Control of NR polymerization using a CS approach. (*A*) Change in extinction spectra of the NRs in the course of their self-assembly for [CS]/[NR] = 0.6 (green line) and [CS]/[NR] = 0 (blue line), t_{SA}= 60 min, C_w = 15 vol %. Black line represents initial extinction spectra of the NRs in both systems at t_{SA} = 0; red line represents extinction spectra of CSs in the DMF–water mixture at C_w = 15 vol % and [CS] = 2.5 nM. (*B*) Variation in $\Delta\lambda_{LSPR}$ of the NRs with self-assembly time for [CS]/[NR] of 0 (■), 0.16 (●), 0.6 (▲), 1.2 (▼), and 1.55 (◀), C_w= 15 vol %. (*C*) Variation in $\overline{X}_n$ of the NR chains with self-assembly time t_{SA} for different [CS]/[NR] ratios. Symbols correspond to experimental results obtained from TEM image analysis; the lines correspond to the predictions of *SI Appendix*, Eq. **S13**. (*D*) Variation in $\overline{X}_n$ of the NR chains with conversion for different [CS]/[NR] ratios, lines correspond to the fit to *SI Appendix*, Eq. **S8**. Symbols in *C* and *D* are the same as those in *B*. Error bars indicate SD.

Experimentally, the model was validated by using the ability to visualize polymer chains, the type of bonds formed in the course of polymerization and the individual NRs and CSs. The distribution in the concentrations of all types of species at a given t_{SA} was modeled using *SI Appendix*, Eqs. **S9–S12**, which allowed the calculation of the rate constants for the formation of all bonds in the system. Fig. 2*C* shows agreement between the experiments and the model (R^2 = 0.986).

Fig. 4 *C* and *D* shows the variation in the predicted and experimental values of $\overline{X}_n$ at a particular self-assembly time t_{SA} and at a particular conversion P_{NR} (defined as the fraction of NR ends reacted at t_{SA}), respectively. The variation of $\overline{X}_n$ at a particular t_{SA} was expressed as

$$\overline{X}_n(t_{SA}) = \frac{1}{1 - \frac{c_{NR-NR}}{c_{NR_0}}}, \quad [1]$$

where c_{NR-NR} is the concentration of NR–NR bonds and c_{NR_0} is the initial concentration of NR ends.

Furthermore, the average degree of polymerization of the NR chains was predicted as

$$\overline{X}_n = \frac{1}{1 - P_{NR} + \frac{1}{2}EP_{CS}\frac{[CS]}{[NR]}}, \quad [2]$$

where P_{NR} and P_{CS} are conversions of NRs and CSs (defined as the fraction of NR ends and CSs, respectively, reacted at t_{SA}), and E is the efficiency of the correct attachment of CSs to the end of the chain calculated as $E = \frac{2}{K(\overline{X}_n - 1) + 2}$ (K is the ratio of reactivities of CSs with respect to the junctions and chain ends). We stress that it is expected theoretically and has been shown experimentally (*SI Appendix*) that the value of E decreases in the course of self-assembly: when the NR chain grows, the probability to find a junction along the chain, instead of chain end, increases. Fitting Eq. **2** to the experimental data for different [CS]/[NR] ratios (Fig. 4*D*) indicated that (*i*) the CSs are less reactive toward junctions than to the ends of the NR chains (K = 0.13 ± 0.06), due to the steric hindrance effect, in agreement with the rate constants found with the kinetic model (*SI Appendix*), and (*ii*) the NRs are more reactive in forming NR–NR bonds, rather than NR–CS bonds (P_{CS}/P_{NR} = 0.44 ± 0.04), due to the predesigned difference in dimensions of reactive patches in CSs and NRs. These findings highlight the importance of the rational design of CSs.

By adding a particular amount of CS at the beginning of the self-assembly process, we fine-tuned the final composition and structure of the nanopolymer (Fig. 4*C*). With a detailed understanding of the polymerization kinetics, one could also quench polymerization by adding CSs, although in a different amount, in the reaction system after a particular self-assembly time t_{SA} (*SI Appendix*). Polymer with the same $\overline{X}_n$ and polydispersity index will be obtained using both approaches depending on the amount and time of addition of the CSs.

In addition to the detailed information about polymerization in the presence of CSs, the experimental and theoretical results presented in our work can be applied to the self-assembly of nanopolymers. Whereas the use of CSs enabled control of the value of $\overline{X}_n$, the theoretical model predicted the ratio [CS]/[NR], at which a particular value of $\overline{X}_n$ is achieved after a particular self-assembly time. These results are important for sensing applications of polymer-like chains of Au NRs, for which a red shift of the longitudinal surface plasmon resonance depends on

chain degree of polymerization (27). Furthermore, efficient surface-enhanced Raman spectroscopy probes benefit from the use of short NR chains with $\overline{X}_n$ of 2–3 (28). For [CS]/[NR] = 1.55, the self-assembly yielded chains with $\overline{X}_n = 2$ in 50 min, after which the value of $\overline{X}_n$ did not change over 24 h.

Conclusions

In summary, this work shows that nanoparticle models enable detailed studies of polymerization reactions, beyond the determination of average degrees of polymerization, and provide guidance in the design of molecules with a particular function. Further steps should exploit recent advances in in situ electron microscopy studies of nanoparticle motion and assembly in solution (29), to gain deeper understanding of the reaction mechanism. On the other hand, our work highlights, again, the applications of the synthetic concepts of polymer chemistry to controllable and quantitative assembly of nanostructures with required properties. Furthermore, the attachment of a colloidal CS to one end of the nanoparticle chain breaks the symmetry of colloidal polymers, thereby paving the way for unique modes of self-assembly, and bringing a different functionality to the chain end.

ACKNOWLEDGMENTS. A.K. thanks I. Gourevich and N. Coombs for help with TEM imaging. E.K., R.M.C., A.K., and H.T.-A. thank Natural Sciences and Engineering Research Council of Canada (Strategic Network Grant and Discovery grant) for financial support of this work. M.R. acknowledges financial support from the National Science Foundation under Grants CHE-0911588, DMR-0907515, DMR-1309892, DMR-1121107, and DMR-1122483, the National Institutes of Health under 1-P5-HL107168, 1-P01-HL108808-01A1, and the Cystic Fibrosis Foundation. A.K. acknowledges an Ontario Trillium Scholarship.

1. Glotzer SC, Solomon MJ (2007) Anisotropy of building blocks and their assembly into complex structures. *Nat Mater* 6(8):557–562.
2. Wei Y, Bishop KJM, Kim J, Soh S, Grzybowski BA (2009) Making use of bond strength and steric hindrance in nanoscale "synthesis". *Angew Chem Int Ed Engl* 48(50): 9477–9480.
3. Guerrero-Martínez A, Grzelczak M, Liz-Marzán LM (2012) Molecular thinking for nanoplasmonic design. *ACS Nano* 6(5):3655–3662.
4. Wang Y, et al. (2012) Colloids with valence and specific directional bonding. *Nature* 491(7422):51–55.
5. Liu K, et al. (2010) Step-growth polymerization of inorganic nanoparticles. *Science* 329(5988):197–200.
6. Gröschel AH, et al. (2012) Precise hierarchical self-assembly of multicompartment micelles. *Nat Commun* 3:710.
7. Bharti B, Findenegg GH, Velev OD (2012) Co-assembly of oppositely charged particles into linear clusters and chains of controllable length. *Sci Rep* 2(1004):1004.
8. Keng PY, Shim I, Korth BD, Douglas JF, Pyun J (2007) Synthesis and self-assembly of polymer-coated ferromagnetic nanoparticles. *ACS Nano* 1(4):279–292.
9. Slaughter LS, et al. (2012) Toward plasmonic polymers. *Nano Lett* 12(8):3967–3972.
10. Yatsui T, et al. (2010) Self-assembly method of linearly aligning ZnO quantum dots for a nanophotonic signal transmission device. *Appl Phys Lett* 96(13):133106.
11. Nakata K, Hu Y, Uzun O, Bakr O, Stellacci F (2008) Chains of superparamagnetic nanoparticles. *Adv Mater* 20(22):4294–4299.
12. Stewart ME, et al. (2008) Nanostructured plasmonic sensors. *Chem Rev* 108(2): 494–521.
13. Neubrech F, et al. (2012) Infrared optical properties of nanoantenna dimers with photochemically narrowed gaps in the 5 nm regime. *ACS Nano* 6(8):7326–7332.
14. Liu N, et al. (2012) Manipulating magnetic plasmon propagation in metallic nanocluster networks. *ACS Nano* 6(6):5482–5488.
15. Odian G (2004) *Principles of Polymerization* (Wiley, New York), 4th Ed.
16. De Greef TFA, et al. (2009) Supramolecular polymerization. *Chem Rev* 109(11): 5687–5754.
17. Knoben W, Besseling NAM, Cohen Stuart MA (2006) Chain stoppers in reversible supramolecular polymer solutions studied by static and dynamic light scattering and osmometry. *Macromolecules* 39(7):2643–2653.
18. Smulders MMJ, et al. (2011) Cooperative two-component self-assembly of mono- and ditopic monomers. *Macromolecules* 44(16):6581–6587.
19. Wolf BA, Willms MM (1978) Measured and calculated solubility of polymers in mixed-solvents-co-non-solvency. *Makromol Chem* 179(9):2265–2277.
20. Nikoobakht B, El-Sayed MA (2003) Preparation and growth mechanism of gold nanorods (NRs) using seed-mediated growth method. *Chem Mater* 15(10):1957–1962.
21. Nie Z, et al. (2007) Self-assembly of metal-polymer analogues of amphiphilic triblock copolymers. *Nat Mater* 6(8):609–614.
22. Yu H, et al. (2005) Dumbbell-like bifunctional Au-Fe3O4 nanoparticles. *Nano Lett* 5(2): 379–382.
23. Leung KC, et al. (2012) Gold and iron oxide hybrid nanocomposite materials. *Chem Soc Rev* 41(5):1911–1928.
24. Xu C, et al. (2008) Au-Fe3O4 dumbbell nanoparticles as dual-functional probes. *Angew Chem Int Ed Engl* 47(1):173–176.
25. Brandrup J, Immergut EH, Grulke EA (1999) *Polymer Handbook* (Wiley, New York), 4th Ed.
26. Su K-H, Wei Q-H, Zhang X (2003) Interparticle coupling effects on plasmon resonances of nanogold particles. *Nano Lett* 3(8):1087–1090.
27. Liu K, et al. (2013) *In situ* plasmonic counter for polymerization of chains of gold nanorods in solution. *ACS Nano* 7(7):5901–5910.
28. Lee A, et al. (2011) Probing dynamic generation of hot-spots in self-assembled chains of gold nanorods by surface-enhanced Raman scattering. *J Am Chem Soc* 133(19): 7563–7570.
29. Liu Y, Lin X-M, Sun Y, Rajh T (2013) In situ visualization of self-assembly of charged gold nanoparticles. *J Am Chem Soc* 135(10):3764–3767.